

# Learning DFT

Peter Schmitteckert  
*HQS Quantum Simulations GmbH*  
*Haid-und-Neu-Straße 7*  
*76131 Karlsruhe*  
*Germany*

(Dated: August 19, 2020)

We present an extension of reverse engineered Kohn-Sham potentials from a density matrix renormalization group calculation towards the construction of a density functional theory functional via deep learning. Instead of applying machine learning to the energy functional itself, we apply these techniques to the Kohn-Sham potentials. To this end we develop a scheme to train a neural network to represent the mapping from local densities to Kohn-Sham potentials. Finally, we use the neural network to up-scale the simulation to larger system sizes.

## I. INTRODUCTION

In the quest of solving strongly interacting quantum systems the density matrix renormalization group technique (DMRG) [1–5] has turned out to be a powerful tool. Representing a many-particle wave function based approach it is perfectly suited to attack strongly interacting many particle problems. However, its downside are the high computational costs, rendering the DMRG being too expensive for large systems. In contrast, the density functional theory (DFT) has proven to be successful in the prediction of structure of molecules, solids and surfaces,[6–8] although it is based on a single particle description only. The DFT is based on the Hohenberg-Kohn theorem [6] which states that the ground state properties of a many-particle system is determined by the local density, specifically, for each observable there exists a functional of the density, which provides the ground state expectation value of the observable, when evaluated with the ground state density. In result the ground state energy functional is minimized by the ground state energy. Within the Kohn-Sham construction [7] one describes an interacting system by a non-interacting system, where the local Kohn-Sham potential  $v_x^{\text{KS}}$  replaces the local potential to mimic the effect of the interaction. Provided the interaction is kept fix there is a one-to-one correspondence between the local potentials and the local densities. Despite this solid foundation of the DFT and decades of research, DFT is unreliable for strongly correlated electron systems, as the nature of the associated functional is unknown. Gunnarson and Schönhammer [9] extended the DFT to a homogeneous lattice system by explicitly reverse engineering the Kohn-Sham potentials of the solution provided by exact diagonalization. This approach was the extended in [10] to inhomogeneous systems, see also [11]. In this work we study the extension of the reverse engineered Kohn-Sham potentials for specific systems to the construction of DFT functionals.

To achieve such a construction we make use of deep learning and neuronal networks (NN), where we refer to the excellent introduction by Nielson[12] and Appendix A. NN have actually a long history, starting with the pioneering work of McCulloch, Warren, and Pitts [13]. The major steps in the development of today's success in pattern recognition consists in the development of the back propagation algorithm [14] and the invention of convolutional networks [15], combined with the computational power provided by graphic cards. In addition, the availability of free software packages[16–18] simplifies the application of neural network enormously.

Machine learning has already a broad application in physical simulations, for a review see[19]. In the context of simulating electronic systems machine learning has been applied to bypass the Schrödinger equation[20, 21]. That is, training the neural network with DFT and post-DFT results in order to predict properties directly. Another approach consists in improving existing DFT functionals for molecules [22–24]. In addition, DFT functionals have been constructed by learning the energy functional.[25–27] Here we are following a different route. Instead of applying machine learning to the energy functional, we apply it to the learning of the Kohn-Sham potentials. The idea of this approach is that it should simplify a divide and conquer approach to larger, even inhomogeneous systems. In addition, there is no problem associated with the functional derivatives of the energy functional, as we are already learning the derivatives.

In this work we look at a one dimensional interacting Fermi system with disorder Eq. (1). The model has been studied for a long time and caught attraction by the work of Giamarchi and Schultz [28], who predicted a phase transition from the Anderson insulator to a metallic Luttinger liquid for attractive interaction,  $U = -1t$ , and weak disorder. For repulsive interaction the interaction enhances the localization induced by the disorder[28, 29] while for strong disorder and interaction the interplay of disorder and charge density wave ordering renders the system complicated[30, 31].

In Section II we introduce the model under investigation and discuss the application of a NN to the system in Section III and the up-scaling is presented in Section IV. In Appendix A we provide a detailed introduction into fitting functions with neural networks and finally sketch an extension using convolutional networks in Appendix B.

## II. THE MODEL

The model under investigation is chosen to be formally simple, but beyond the reach of standard DFT functionals. To this end we look at spinless fermions in one dimension, with a nearest neighbor hopping  $t = 1$ , periodic boundary conditions (PBC), nearest neighbor interaction  $U$  and a strong onsite disorder  $v_x$ ,

$$\mathcal{H} = \underbrace{-t \sum_x \hat{c}_{x-1}^\dagger \hat{c}_x + \hat{c}_x^\dagger \hat{c}_{x-1}}_{\text{kinetic part}} + \underbrace{U \sum_x \hat{n}_{x-1} \hat{n}_x}_{\text{interaction}} + \underbrace{\sum_x v_x \hat{n}_x}_{\text{disorder}}. \quad (1)$$

Here,  $\hat{c}_x^\dagger$  ( $\hat{c}_x$ ) denote the fermionic creation (annihilation) operator at site  $x$ ,  $\hat{n}_x = \hat{c}_x^\dagger \hat{c}_x$  the local density, and  $M = 98$  the number of lattice sites. The interaction is chosen to be  $U = 1.0$ , and the disorder potentials  $v_x$  is chosen from a

uniform distribution between  $\pm W/2$ , and smoothed with a cosine filter with a width of 3 three sites. Specifically, we choose  $\epsilon_x \in [-W/2, W/2]$  uniformly distributed and obtain the smoothed potentials from

$$v_x = \sum_{s=-d}^{s=d} \cos^2\left(\frac{s\pi}{2d+2}\right) \frac{\epsilon_{x+s}}{\sqrt{d+1}} \quad (2)$$

with  $d = 3$  and  $W = 2$ . The reason for the smoothing is that disorder typically stems from scatterer in the substrate. So each scatterer should also effect neighboring sites. From test runs with fewer samples than provided below, but without the smoothing, we conclude that it doesn't alter the findings of this work.

In order to obtain the reference data for training the network we perform a sample statistics using the density matrix renormalization group technique where we used the ‘‘safety belt’’ approach as explained in [32, 33] to avoid getting trapped in an excited state during the DMRG initialization.

### III. NEURAL NETWORK AS A GENERATOR OF DFT POTENTIALS

From each DMRG run we obtain the local density  $n_x$ . We then perform an inverse DFT [9–11, 34, 35], where we search for a non interacting Hamiltonian,

$$\mathcal{H}_0 = \underbrace{-t \sum_x \hat{c}_{x-1}^\dagger \hat{c}_x + \hat{c}_x^\dagger \hat{c}_{x-1}}_{\text{kinetic part}} + \underbrace{\sum_x v_x^{\text{KS}} \hat{n}_x}_{\text{Kohn-Sham potential}}, \quad (3)$$

that is we search numerically for the Kohn-Sham potential  $v_x^{\text{KS}}$ , such that

$$\langle \hat{n}_x \rangle_{\mathcal{H}} = \langle \hat{n}_x \rangle_{\mathcal{H}_0}. \quad (4)$$

In return we obtain for each disorder realization  $\{v_x\}$  the corresponding Kohn-Sham potentials  $v_x^{\text{KS}}$ . By building an infinite table listing the Kohn-Sham potential for every possible disorder configuration we would obtain the full DFT functional for this system. Since this is not feasible we explore the possibility of using a NN to construct such a functional. We would like to remark, that we are actually constructing the Kohn-Sham potentials and the energy functional is given by solving the Kohn-Sham system.

At a first sight it looks rather boring to construct a DFT functional for a system that one has already solved using the DMRG. The main reason for this work is that we would like to apply the functional constructed in this section for larger systems, i.e. to perform an up-scaling in system size, see Sec. IV.

In our setup we constructed a set of training and test data by performing an ensemble statistics for 14.950 systems for the training set, and 50 realizations for the testing set, where the testing set was never used as a training input. All simulations are performed at half filling. In order to avoid getting stuck at an excited state during the DMRG sweeping we added the ground state of a homogeneous, delocalised systems to the density matrix used for the selection of the target space.[29, 30, 32] The reason for this approach is explained in detail in [32]. In addition we targeted for the three states lowest in energy in an initial run, performed three finite lattice sweeps and kept at least 400 states per block, while we increased the number of states per block to ensure a discarded entropy below  $10^{-5}$ . We then restarted each run keeping at least 450 states per block, targeting for the two states lowest in energy and performing three sweeps and ensured a discarded entropy below  $10^{-6}$ . Finally we restarted each run again, keeping at least 500 states per block, targeting the ground state only, performed seven finite lattice sweeps and increased the number of states kept per block to ensure a discarded entropy below  $10^{-8}$ .

For each sample the calculated the corresponding Kohn-Sham potentials  $v_x^{\text{KS}}$ . For each site  $x$  of a system we constructed a data set consisting of the densities starting  $s = 35$  sites left to  $x$  up to the densities for the  $s$  sites right of  $x$ , employing PBC,

$$\{n_{x-s}, n_{x-s+1}, \dots, n_{x+s}\} \longrightarrow v_x^{\text{KS}} \quad (5)$$

mapping each set of densities to the corresponding Kohn-Sham potential  $v_x^{\text{KS}}$ . We didn't use the complete set of  $M = 98$  densities as we later want to use the data for up-scaling and we wanted to avoid targeting at precisely  $M = 98$  sites. We therefore obtain  $98 * 14.950 = 1.465.100$  training sets Eq. (5) and  $98 * 50 = 4.900$  testing sets Eq. (5) with an input length of  $71 = 2 * 35 + 1$  and a single valued result. We applied a tanh activation and therefore re-scaled the input densities by  $2(n_x - 0.5)$ . The network used has a  $71 \times 251 \times 249 \times 1$  structure, that is 71 input values, namely the densities, one output values, the Kohn-Sham potential, two hidden layers consisting of 251 and

249 neurons. We have performed tests with other layouts, especially with deeper networks. The results obtained with those networks were very similar to ones presented below.

For details on how to fit functions with NN we refer to appendix A.

We trained the network first by using the `tiny DNN` [16] software package and switched later to `tensorflow` [17] with the `Keras` [18] interface. During the training phase we tried various available optimizer, most notably stochastic gradient descent (SGD) [36], adaptive moment estimation (Adam) [37], and the adaptive gradient algorithm Adagrad [38]. In this section we are only reporting the results for the optimization run with the lowest deviation which we achieved using `tiny DNN`.

In addition to the Kohn-Sham potentials  $v_x^{\text{KS}}$  we are also defining the Hartree exchange correlations potentials  $v_x^{\text{HXC}}$

$$v_x^{\text{HXC}} = v_x^{\text{KS}} - v_x \quad (6)$$

that is, the interaction induced change of the local potential. Note that in the non-interacting limit,  $U = 0$ , the Hartree exchange correlation potential is zero by definition. We did not subtract the Hartree contribution from  $v_x^{\text{HXC}}$  as the Hartree-Fock approximation has problems for strongly correlated one-dimensional systems, see [11].

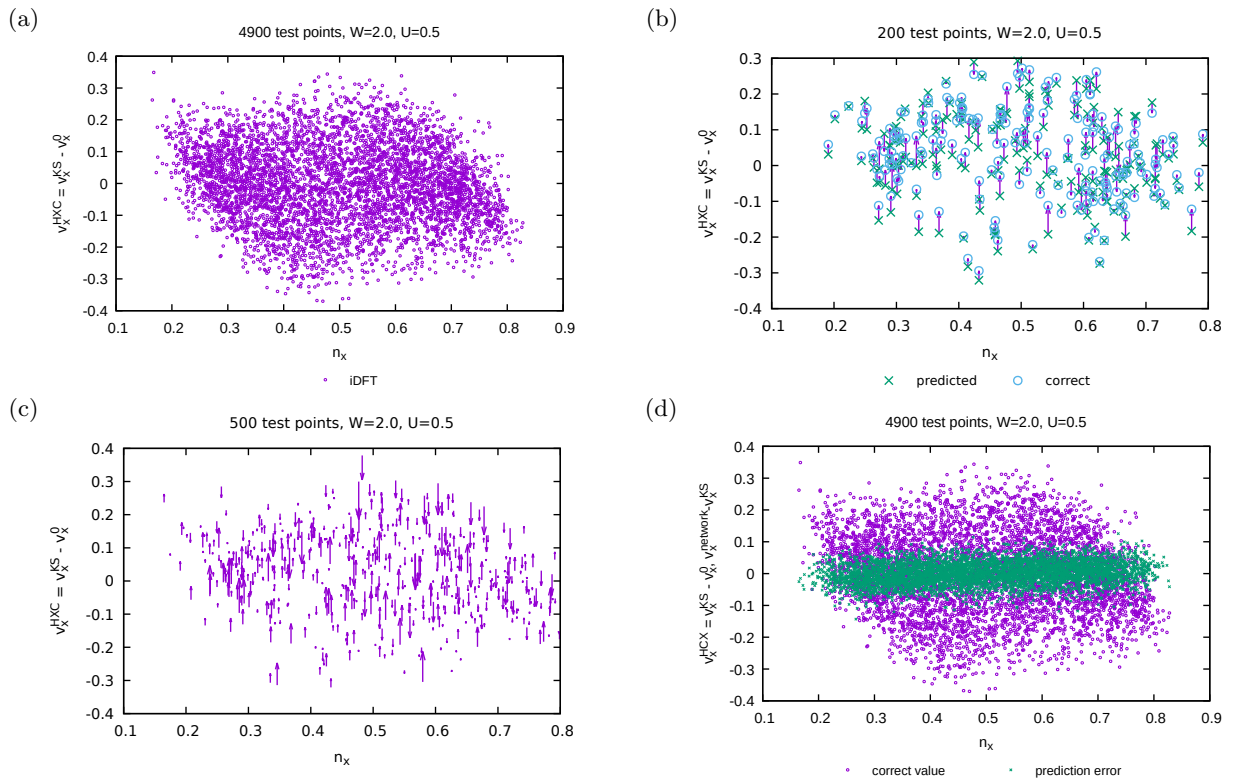


FIG. 1. Results for the NN based DFT: (a) interaction induced  $v^{\text{HXC}}$  for the test data vs. the local density; (b) The  $v^{\text{HXC}}$  potentials for 200 test values, the corresponding from the NN predicted values and arrows indicating the errors; (c) the error arrows for 500 test values; (c) circles: the cloud of  $v^{\text{HXC}}$  potentials as in Fig. 1a, crosses: the error in the predicted Kohn-Sham values.

In Fig. 1a we show the  $v^{\text{HXC}}$  potentials vs. the local density. Just by looking at the plot it is obvious that any local density approximation will not be able to describe the Kohn-Sham potentials. It is also hard to imagine that any density gradient based expansion will be able to represent the rather dense cloud of potentials. The key point in local density approximations (LDA) and gradient based expansions consists in assuming that the density functional is smooth on short wave lengths and that one can expand the functional around its local value. In contrast the  $v^{\text{HXC}}$  potentials as shown in Fig. 1a are highly oscillating and multi valued. Even if one doesn't require a smooth density dependence of the  $v^{\text{HXC}}$  potentials one would need a least a strongly quenched distribution in order to construct an LDA based approximation.

Fig. 1b compares the correct  $v^{\text{HXC}}$  potentials with the ones predicted from the NN for the first 200 testing sets, where the arrows denote the error of the prediction. In Fig. 1c we display the same data, just drawing the arrows for the errors for the first 500 testing sets. Here, for each sample the error arrows start at the predicted value and end at

the desired correct value. Finally in Fig. 1d we show the cloud of  $v^{\text{HXC}}$  potentials for the complete testing set as in Fig. 1a. In addition we also show the difference between the  $v^{\text{KS}}$  as predicted from the NN minus the non-interaction potential. If the NN would work perfectly, those values should zero.

At a first sight the results look rather disappointing. The NN is only capable to partially capture the interaction induced  $v^{\text{HXC}}$  potentials. However, one should take into account that hand-crafting a density functional that reconstruct the cloud as displayed Fig. 1a is presumably impossible.

To make this result quantitative we show in Fig. 2a the distribution function of the  $v^{\text{HXC}}$  potentials in comparison to the error of the predicted Kohn-Sham potentials, where both distributions can be fit by a Gaussian distribution. The width of  $\sigma = 0.13$  for the  $v^{\text{HXC}}$  is to be contrasted to the width of  $\sigma = 0.0347$  of the distribution of the errors of the NN. Therefore, the NN is capable to capture about 73% of the interaction effects. While one would like to have a better agreement, the results shows that most of the correlations are already incorporated and the NN might be able to provide correct trends.

One may try to improve the results by constructing more sophisticated NN. However, within this work we didn't succeed, see Appendix B. We also note that it is straightforward to extract the total energy and the single particle gap from the inverse DFT calculations, see [10, 11], which could be incorporated into the output of the NN.

#### IV. UP-SCALING

In this section we address the question whether we can use the approach to up-scale the calculations for larger system sizes, i.e. using the NN trained from the  $M = 98$  site systems to obtain results for larger systems. To this end we performed DMRG runs for ten  $M = 250$  site systems using the same DMRG parameter/setup as in Sec. III, and extracted 2500 test sets as outlined in Eq. (5). In Fig. 2b we compared the error of the Kohn-Sham potentials for the 250 site system obtained from the NN trained with the  $M = 98$  sites data. Interestingly the width of the error

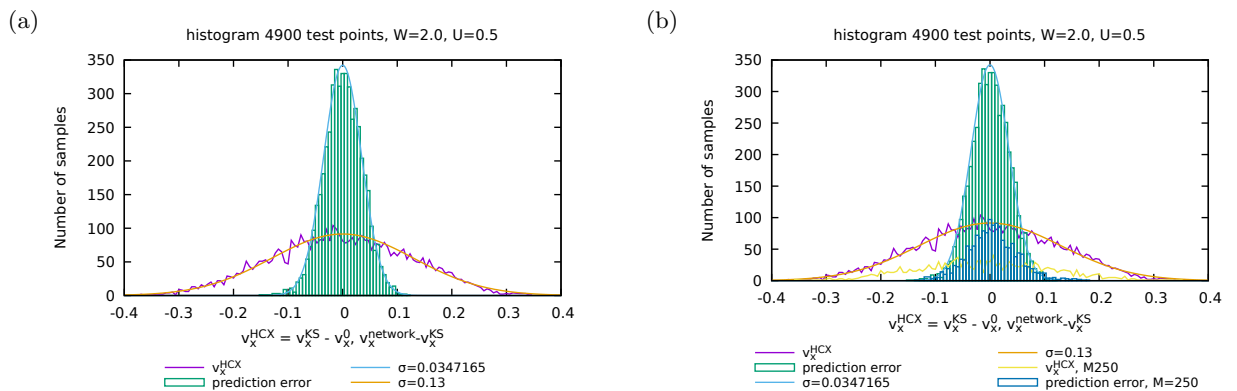


FIG. 2. The error distribution of the NN: (a) The distribution of the  $v^{\text{HXC}}$  potentials and the distribution of the error in the prediction of the  $v^{\text{KS}}$  potentials for the 98 site system and the corresponding Gaussian fits. (b) The same data as in (a) combined with the results obtained from up-scaling the NN to 250 sites.

distribution does not increase. The result therefore suggests that the up-scaling of an NN trained on small systems to an evaluation on larger systems is a fruitful concept.

#### V. SUMMARY

In this work we applied the concept of deep learning via neural networks with the reverse engineering of Kohn-Sham potentials in order to construct a DFT functional by learning the Kohn-Sham potentials. We applied the idea to systems of one-dimensional spinless fermions with nearest neighbor interaction and hopping combined with on-site disorder. We showed, while being not perfect, we managed to capture 73% of the interaction induced exchange correlation potentials. In addition, we demonstrated that the concept of constructing functionals for the Kohn-Sham potentials from small system and to apply them for larger systems is a promising route for the investigation of interacting Fermi systems.

## ACKNOWLEDGMENTS

Most of the work reported here was performed while being at the university of Würzburg and was supported by ERC-StG-Thomale-TOPOLECTRICS-336012 and was presented at the FQMT'19 in Prague. We would like to thank Florian Eich for insightful discussions.

All authors contributed equally to the manuscript and the acquisition of the results.

- 
- <sup>1</sup> Steven R. White. Density matrix formulation for quantum renormalization groups. *Phys. Rev. Lett.*, 69:2863–2866, Nov 1992. doi:10.1103/PhysRevLett.69.2863. URL <http://link.aps.org/doi/10.1103/PhysRevLett.69.2863>.
- <sup>2</sup> S. R. White and R. M. Noack. Real-space quantum renormalization groups. *Phys. Rev. Lett.*, 68:3487–3490, Jun 1992. doi:10.1103/PhysRevLett.68.3487. URL <http://link.aps.org/doi/10.1103/PhysRevLett.68.3487>.
- <sup>3</sup> Steven R. White. Density matrix renormalization group. *Phys. Rev. B*, 48:10345, 1993.
- <sup>4</sup> Reinhard M. Noack and Salvatore R. Manmana. Diagonalization- and numerical renormalization-group-based methods for interacting quantum systems. In Adolfo Avella and Ferdinando Mancini, editors, *LECTURES ON THE PHYSICS OF HIGHLY CORRELATED ELECTRON SYSTEMS IX: Ninth Training Course in the Physics of Correlated Electron Systems and High-Tc Superconductors*, volume 789, pages 93–163, Salerno, Italy, 2005. AIP.
- <sup>5</sup> Karen A. Hallberg. New trends in density matrix renormalization. *Adv. Phys.*, 55(5):477–526, 2006. doi: <http://dx.doi.org/10.1080/00018730600766432>.
- <sup>6</sup> P. Hohenberg and W. Kohn. Inhomogeneous electron gas. *Phys. Rev.*, 136:B864–B871, Nov 1964. doi: 10.1103/PhysRev.136.B864. URL <https://link.aps.org/doi/10.1103/PhysRev.136.B864>.
- <sup>7</sup> W. Kohn and L. J. Sham. Self-consistent equations including exchange and correlation effects. *Phys. Rev.*, 140:A1133–A1138, Nov 1965. doi:10.1103/PhysRev.140.A1133. URL <https://link.aps.org/doi/10.1103/PhysRev.140.A1133>.
- <sup>8</sup> R.M. Dreizler and E.K.U. Gross. *Density Functional Theory*. Springer–Verlag, 1990.
- <sup>9</sup> O. Gunnarsson and K. Schönhammer. Density-functional treatment of an exactly solvable semiconductor model. *Phys. Rev. Lett.*, 56(18):1968–1971, May 1986. doi:10.1103/PhysRevLett.56.1968.
- <sup>10</sup> Peter Schmitteckert and Ferdinand Evers. Exact ground state density-functional theory for impurity models coupled to external reservoirs and transport calculations. *Phys. Rev. Lett.*, 100(8):086401, Feb 2008. doi:10.1103/PhysRevLett.100.086401.
- <sup>11</sup> Peter Schmitteckert. Inverse mean field theories. *Phys. Chem. Chem. Phys.*, 20:27600–27610, 2018. doi: 10.1039/C8CP03763A. URL <http://dx.doi.org/10.1039/C8CP03763A>.
- <sup>12</sup> Michael A. Nielsen. *Neural Networks and Deep Learning*. Determination Press, 2015.
- <sup>13</sup> Warren S. McCulloch and Walter Pitts. A logical calculus of the ideas immanent in nervous activity. *The bulletin of mathematical biophysics*, 5(4):115–133, Dec 1943. ISSN 1522-9602. doi:10.1007/BF02478259. URL <https://doi.org/10.1007/BF02478259>.
- <sup>14</sup> D. E. Rumelhart, Hinton G. E., and R. J. William. Learning representations by back-propagating errors. *Nature*, 323:533, 1986.
- <sup>15</sup> Y LeCun and Y Bengio. Convolutional networks for images, speech, and time series. *The handbook of brain theory and neural networks*, 3361:3539, 1995.
- <sup>16</sup> Taiga Nomi and et.al. tiny dnn.
- <sup>17</sup> Martín Abadi, Ashish Agarwal, Paul Barham, Eugene Brevdo, Zhifeng Chen, Craig Citro, Greg S. Corrado, Andy Davis, Jeffrey Dean, Matthieu Devin, Sanjay Ghemawat, Ian Goodfellow, Andrew Harp, Geoffrey Irving, Michael Isard, Yangqing Jia, Rafal Jozefowicz, Lukasz Kaiser, Manjunath Kudlur, Josh Levenberg, Dandelion Mané, Rajat Monga, Sherry Moore, Derek Murray, Chris Olah, Mike Schuster, Jonathon Shlens, Benoit Steiner, Ilya Sutskever, Kunal Talwar, Paul Tucker, Vincent Vanhoucke, Vijay Vasudevan, Fernanda Viégas, Oriol Vinyals, Pete Warden, Martin Wattenberg, Martin Wicke, Yuan Yu, and Xiaoqiang Zheng. TensorFlow: Large-scale machine learning on heterogeneous systems, 2015. URL <https://www.tensorflow.org/>. Software available from tensorflow.org.
- <sup>18</sup> Francois Chollet et al. Keras, 2015.
- <sup>19</sup> Giuseppe Carleo, Ignacio Cirac, Kyle Cranmer, Laurent Daudet, Maria Schuld, Naftali Tishby, Leslie Vogt-Maranto, and Lenka Zdeborová. Machine learning and the physical sciences. *Rev. Mod. Phys.*, 91:045002, Dec 2019. doi: 10.1103/RevModPhys.91.045002. URL <https://link.aps.org/doi/10.1103/RevModPhys.91.045002>.
- <sup>20</sup> Felix Brockherde, Leslie Vogt, Li Li, Mark E. Tuckerman, Kieron Burke, and Klaus-Robert Müller. Bypassing the kohn-sham equations with machine learning. *Nature Communications*, 8(1):872, Oct 2017. ISSN 2041-1723. doi:10.1038/s41467-017-00839-3. URL <https://doi.org/10.1038/s41467-017-00839-3>.
- <sup>21</sup> Brian Kolb, Levi C. Lentz, and Alexie M. Kolpak. Discovering charge density functionals and structure-property relationships with prophet: A general framework for coupling machine learning and first-principles methods. *Scientific Reports*, 7(1):1192, Apr 2017. ISSN 2045-2322. doi:10.1038/s41598-017-01251-z. URL <https://doi.org/10.1038/s41598-017-01251-z>.
- <sup>22</sup> L. Hu, X. Wang, L. Wong, and G. Chen. Combined first-principles calculation and neural-network correction approach for heat of formation. *J. Chem. Phys.*, 119:11501, 2003.
- <sup>23</sup> Xiao Zheng, LiHong Hu, XiuJun Wang, and GuanHua Chen. A generalized exchange-correlation functional: the neural-networks approach. *Chemical Physics Letters*, 390(1):186 – 192, 2004. ISSN 0009-2614. doi:<https://doi.org/10.1016/j.cplett.2004.04.020>. URL <http://www.sciencedirect.com/science/article/pii/S0009261404000200>.

- S0009261404005603.
- <sup>24</sup> Qin Liu, JingChun Wang, PengLi Du, LiHong Hu, Xiao Zheng, and GuanHua Chen. Improving the performance of long-range-corrected exchange-correlation functional with an embedded neural network. *The Journal of Physical Chemistry A*, 121(38):7273–7281, 2017. doi:10.1021/acs.jpca.7b07045. URL <https://doi.org/10.1021/acs.jpca.7b07045>. PMID: 28876064.
- <sup>25</sup> John C. Snyder, Matthias Rupp, Katja Hansen, Klaus-Robert Müller, and Kieron Burke. Finding density functionals with machine learning. *Phys. Rev. Lett.*, 108:253002, Jun 2012. doi:10.1103/PhysRevLett.108.253002. URL <https://link.aps.org/doi/10.1103/PhysRevLett.108.253002>.
- <sup>26</sup> John C. Snyder, Matthias Rupp, Katja Hansen, Leo Blooston, Klaus-Robert Müller, and Kieron Burke. Orbital-free bond breaking via machine learning. *The Journal of Chemical Physics*, 139(22):224104, 2013. doi:10.1063/1.4834075. URL <https://doi.org/10.1063/1.4834075>.
- <sup>27</sup> Li Li, Thomas E. Baker, Steven R. White, and Kieron Burke. Pure density functional for strong correlation and the thermodynamic limit from machine learning. *Phys. Rev. B*, 94:245129, Dec 2016. doi:10.1103/PhysRevB.94.245129. URL <https://link.aps.org/doi/10.1103/PhysRevB.94.245129>.
- <sup>28</sup> T. Giamarchi and H. J. Schulz. Anderson localization and interactions in one-dimensional metals. *Phys. Rev. B*, 37:325–340, Jan 1988. doi:10.1103/PhysRevB.37.325. URL <https://link.aps.org/doi/10.1103/PhysRevB.37.325>.
- <sup>29</sup> P. Schmitteckert, T. Schulze, C. Schuster, P. Schwab, and U. Eckern. Anderson localization versus delocalization of interacting fermions in one dimension. *Phys. Rev. Lett.*, 80:560–563, Jan 1998. doi:10.1103/PhysRevLett.80.560. URL <https://link.aps.org/doi/10.1103/PhysRevLett.80.560>.
- <sup>30</sup> Peter Schmitteckert, Rodolfo A. Jalabert, Dietmar Weinmann, and Jean-Louis Pichard. From the fermi glass towards the mott insulator in one dimension: Delocalization and strongly enhanced persistent currents. *Phys. Rev. Lett.*, 81:2308–2311, Sep 1998. doi:10.1103/PhysRevLett.81.2308. URL <https://link.aps.org/doi/10.1103/PhysRevLett.81.2308>.
- <sup>31</sup> Rodolfo A Jalabert, Dietmar Weinmann, and Jean-Louis Pichard. Partial delocalization of the ground state by repulsive interactions in a disordered chain. *Physica E: Low-dimensional Systems and Nanostructures*, 9(3):347 – 351, 2001. ISSN 1386-9477. doi:[https://doi.org/10.1016/S1386-9477\(00\)00226-5](https://doi.org/10.1016/S1386-9477(00)00226-5). URL <http://www.sciencedirect.com/science/article/pii/S1386947700002265>. Proceedings of an International Workshop and Seminar on the Dynamics of Complex Systems.
- <sup>32</sup> Peter Schmitteckert. Disordered one-dimensional fermi systems. In *Density Matrix Renormalization[33]*, pages 345–355, 1999. ISBN 978-3-540-66129-0.
- <sup>33</sup> I. Peschel, X. Wang, M.Kaulke, and K. Hallberg, editors. *Density Matrix Renormalization*, 1999. ISBN 978-3-540-66129-0.
- <sup>34</sup> K. Schönhammer, O. Gunnarsson, and R. M. Noack. Density-functional theory on a lattice: Comparison with exact numerical results for a model with strongly correlated electrons. *Phys. Rev. B*, 52:2504–2510, Jul 1995. doi:10.1103/PhysRevB.52.2504. URL <https://link.aps.org/doi/10.1103/PhysRevB.52.2504>.
- <sup>35</sup> Ferdinand Evers and Peter Schmitteckert. Density functional theory with exact xc-potentials: Lessons from dmrg-studies and exactly solvable models. *Phys. Status Solidi B*, 250:2330, 2013.
- <sup>36</sup> Herbert Robbins and Sutton Monro. A stochastic approximation method. *Ann. Math. Statist.*, 22(3):400–407, 09 1951. doi:10.1214/aoms/1177729586. URL <https://doi.org/10.1214/aoms/1177729586>.
- <sup>37</sup> Diederik P. Kingma and Jimmy Ba. Adam: A method for stochastic optimization, 2014.
- <sup>38</sup> John Duchi, Elad Hazan, and Yoram Singer. Adaptive subgradient methods for online learning and stochastic optimization. *JMLR*, 12:2121–2159, 2011.

## Appendix A: Neural networks for fitting functions

The main application of neural networks consists in the classification of input variables, i.e. one maps the input to a discrete set of output variable, with the standard internet example of “*is it a cat or not?*”. Here we provide an example for applying a neural network on fitting a function.

### 1. The network

The basic building block of a neural network (NN) consists of a neuron as depicted in Fig. 3a.

The neuron consist of an input  $\{x_i\}$ , weight factors  $\{w_i\}$ , an offset  $b$ , a so-called activation function  $\sigma(z)$ , see Fig. 3b, and the output  $z$ :

$$z = \sigma \left( b + \sum_{\ell} w_{\ell} x_{\ell} \right) \quad (\text{A1})$$

Throughout this work we have always used an tanh activation function. One now combines many neurons, Fig. 3a, into a neural network in a layered fashion by connecting inputs of the neurons of one layer with the outputs of the neurons of the previous layer, see Fig. 4. Since from a user perspective the NN in Fig. 4 translates the input of the first layer into the output of the last layer one calls the first layer the *input* layer, the last one the *output* layer and the other layers are denoted as *hidden* layers. If each neuron is connected to each neuron of the previous layer one

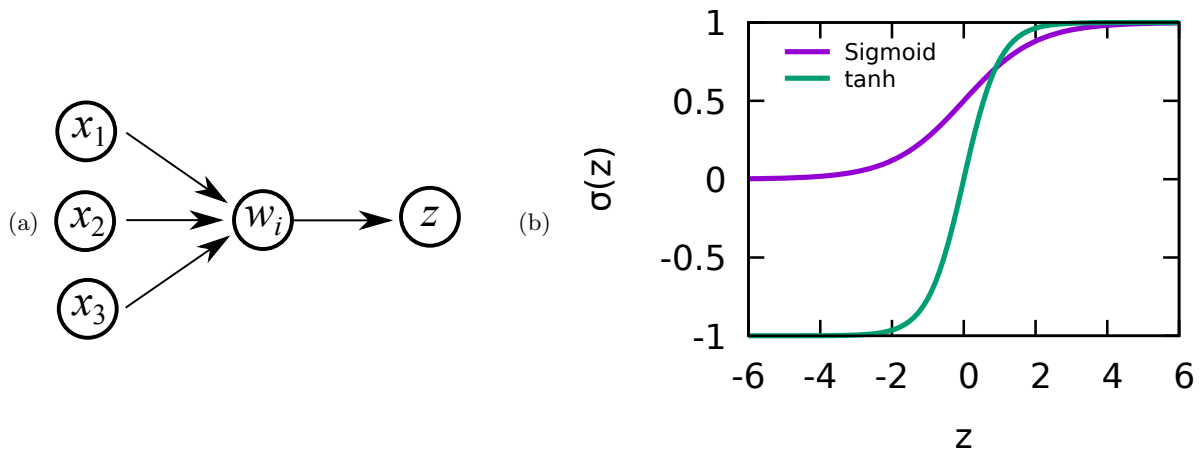


FIG. 3. The building block of a NN: (a) a neuron (b) typical weight function: a sigmoid and a tanh.

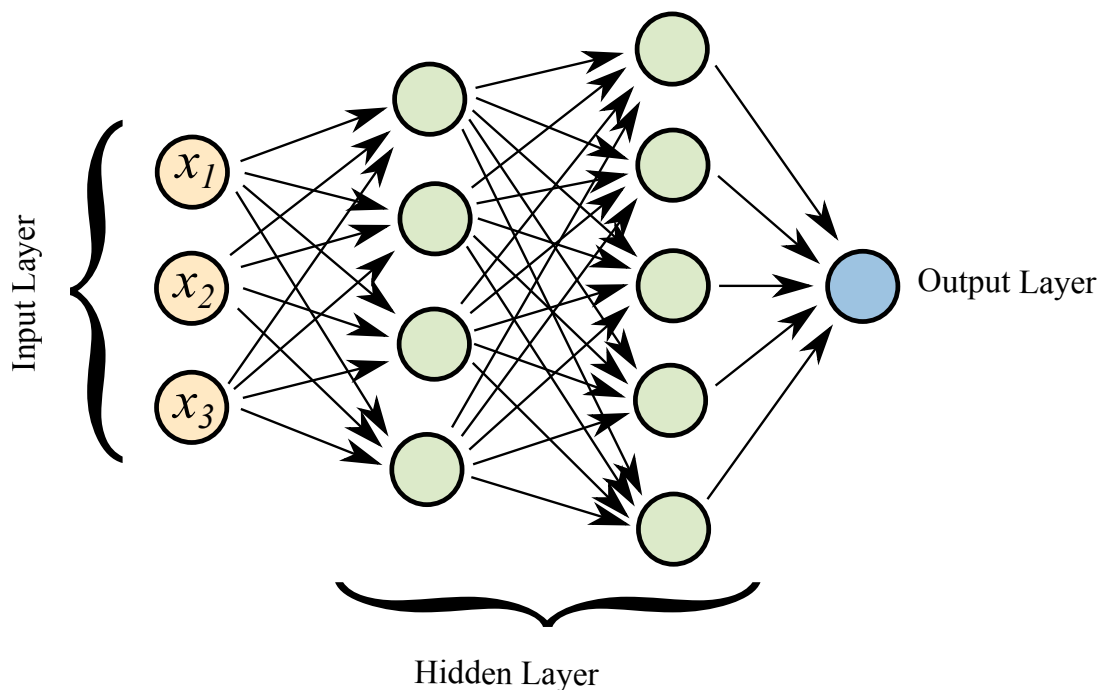


FIG. 4. A neural network build out of neurons shown in Fig. 3a.

calls the network *dense*. The training of a NN is often referred to as machine learning, and in the presence of many hidden layer as deep learning.

In summary, the NN in Fig. 4 calculates an output  $z$  from the input  $\{x_j\}$ , where one has to specify the parameter in Eq. (A1) for each neuron  $n$  in layer  $\ell$ ,

$$z_{\ell,n} = \sigma \left( b_{\ell,n} + \sum_j w_{\ell,n,j} x_j \right). \quad (\text{A2})$$

Of course, this can be extended to create multiple output variables  $z_k$  in the output layer.

In order to apply a NN for fitting functions  $f(x)$  we use a NN with a single input  $x$  and a single output  $z$ . The free parameter  $\{b_{\ell,n}, w_{\ell,n,j}\}$  are the set of fitting parameter. We would like to note that this approach is in contrast



to the desired approach in physics, where one tries to fit a phenomenon with a suitable function using as few fitting parameters as possible. Instead, here we take the opposite approach by using a simple fitting function unrelated to the problem and fit the desired function with a large number of parameters and a few steps of recursion.

## 2. Training the neural network: Minimize Cost Function

The idea to determine the fit parameters for fitting a function  $f(\mathbf{x})$  consists in minimizing a cost function, typically

$$C(\mathbf{x}) = \frac{1}{N} \sum_{i=1}^N \|f(\mathbf{x}_i) - z_{\{b_{\ell,n}, w_{\ell,n,j}\}}(\mathbf{x}_i)\|_2 \quad (\text{A3})$$

where  $N$  denotes the number of training samples. Eq. (A3) could in principle be minimized by a standard steepest descent gradient search. However, due to the vast amount of fit parameters this is not feasible in non-trivial examples, as the number of parameters, and therefore the dimensions of the associated matrices get too large. The breakthrough for neural networks was provided by the invention of the backpropagating algorithm [14] combined with a stochastic evaluation of the gradients [36–38] combined with the massive computational power of graphic cards, and for pattern recognition the use of convolutional layers [15], see below. In the example provided in this section we used `tensorflow` [17] software package combined with the `keras` [18] front end.

## 3. An example

As an example we look at the function

$$f(x) = \sin(3x) - 0.8 \cos^2(13x)e^{0.5x} + 4e^{-\frac{x^2}{0.0005}} + 6e^{-\frac{(x+0.4)^2}{0.0001}} \quad (\text{A4})$$

which has no deeper meaning, it was just handcrafted to represent a not too trivial function combining sharp and non-sharp features.

Since  $f$  is a single valued single argument function the input and output layer consists of a single neuron only. In Fig. 5 we show the results for fitting the function  $f(x)$  in Eq. (A4) with two hidden layers consisting of fifty neurons each. In result we applied a dense NN with a  $1 \times 50 \times 50 \times 1$  structure. In order to train the system we generated 25,000 random values  $x_j$  with the corresponding  $z_j = f(x_j)$ . We then trained the NN by performing a stochastic gradient descent search (SGD) with ten repetitions over the complete set of  $\{x_j, z_j\}$ . We then evaluate the NN on an equidistantly spaced set of  $\{x_\ell\}$ . As one can see in Fig. 5a the result is a rather smooth function that misses the sharp features. The way to improve the NN consists in learning harder, that is, we increased the repetitions of the SGD to 100, Fig. 5b, and 1000, Fig. 5c, which finally leads to a good representation of the functions.

A different strategy consists in using different gradient search strategies, i.e. a different optimizer to minimize the cost function Eq. (A3). In Fig. 5d we show the results where we used only 500 repetitions, however we switched between a SGD and an ADAM optimizer, which performs much better, than just an SGD alone. We would like to remark that a priori it is not clear which optimizer is the best, and the optimizer performance seems to be rather problem dependent, see [12].

Finally in Fig. 6 we present results obtained from a deeper network consisting of  $1 \times 250 \times 50 \times 50 \times 1$  neurons. On the right axis we show the actual error of the fit which is below  $5 \cdot 10^{-3}$  over the complete range. In result we obtained results a rather good approximation to the function at the expense of using more than 15,000 fit parameters  $\{b_{\ell,n}, w_{\ell,n,j}\}$ .

We would like to point out that the approach of using 15,000 fit parameters may appear odd as it renders an understanding of the network impossible. However, we are using the approach to construct a DFT functional. For the latter it is also fair to state that most users of the modern sophisticated DFT functionals have no understanding on the details of their construction.

## Appendix B: A convolutional network

We also tested the setup of a convolutional network. There, in addition to full layer, one constructs a small kernel layer that gets convoluted with the output of another layer. For details we refer to [12].

Specifically we implemented the a NN as displayed in Fig. 7, which resulted into 100,628 fit parameters. However, despite all the effort we could not improve on the results obtained from the (smaller) dense network.

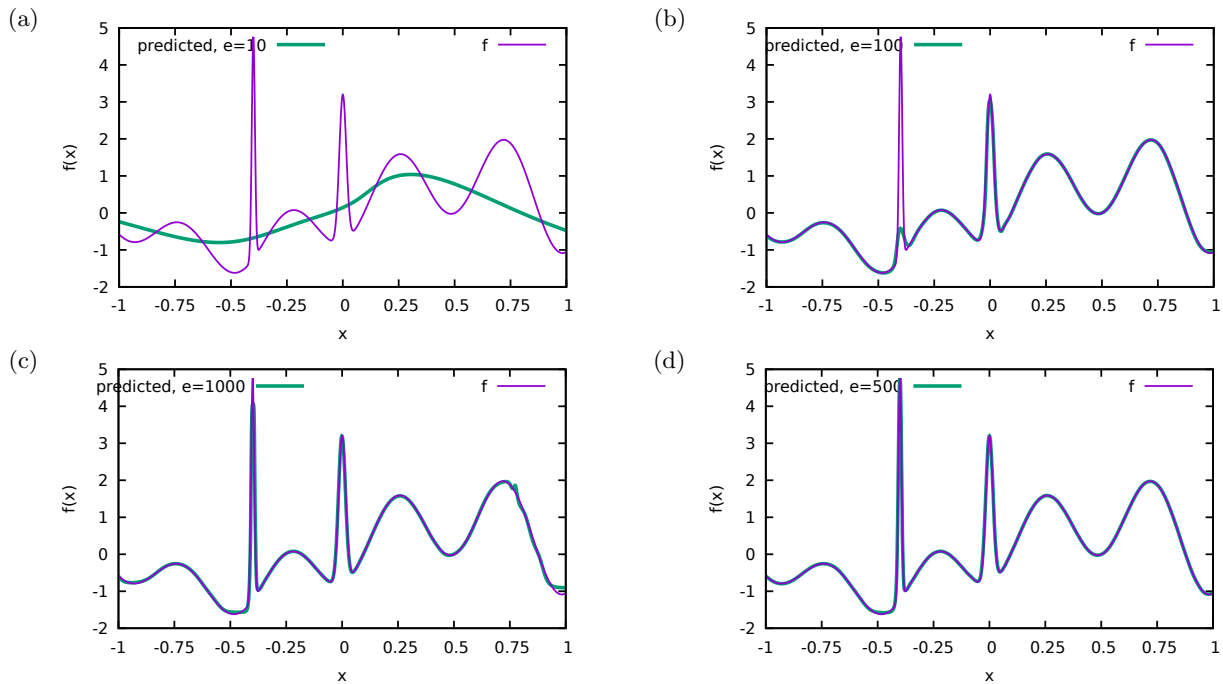


FIG. 5. Fits for the function  $f(x)$  Eq. (A4) using a tanh activation function obtained using `tensorflow/keras` for a  $1 \times 50 \times 50 \times 1$  network. (a) 25.000 samples, 10 repetitions of SGD; (b) 25.000 samples, 100 repetitions of SGD; (c) 25.000 samples, 1000 repetitions of SGD; (d)  $2 \times 25.000$  samples, 250 repetitions ( $1 \times$  SGD &  $1 \times$  ADAM).

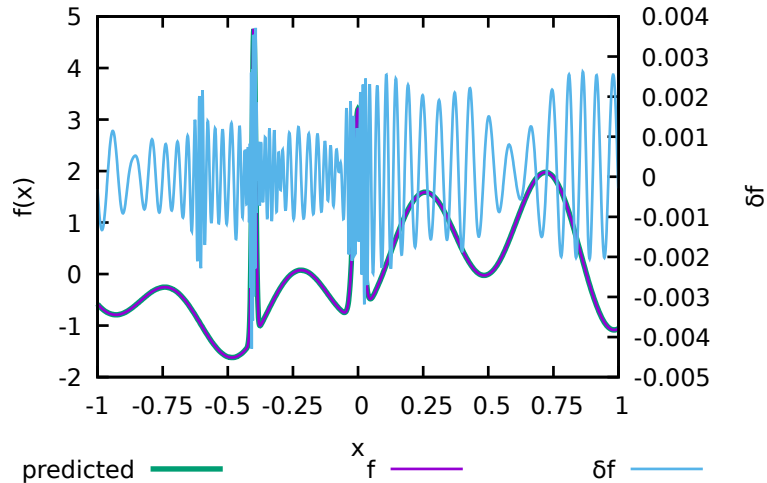


FIG. 6. Fits for the function  $f(x)$  Eq. (A4) using a tanh activation function obtained using `tensorflow/keras` for a  $1 \times 250 \times 50 \times 50 \times 1$  network, 250 repetitions, (SGD & ADAM).

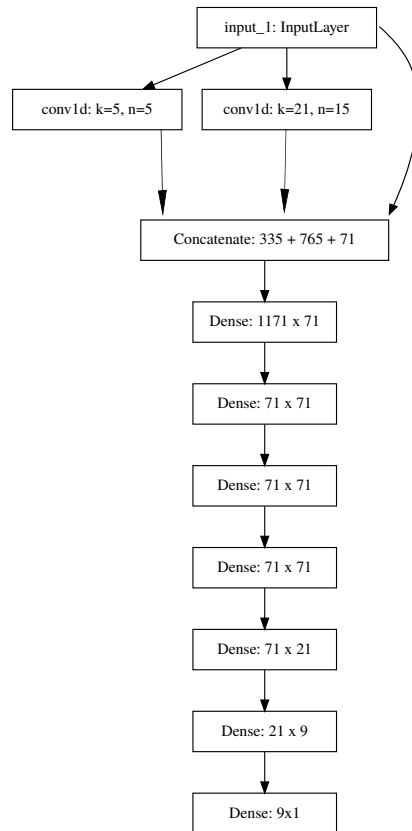


FIG. 7. Layout for the convolutional network. The input layer is connected to two convolutional layer, which are then combined with the input layer to serve for the input of seven hidden full layers.